ACCEPTED MANUSCRIPT

An advanced Wigner-Ville time-frequency analysis of lamb waves signals based upon AR model for efficient damage inspection

To cite this article before publication: Syed Haider Rizvi *et al* 2021 *Meas. Sci. Technol.* in press https://doi.org/10.1088/1361-6501/abef3c

Journal **XX** (XXXX) XXXXXX

An Advanced Wigner-Ville Time-Frequency Analysis of Lamb Waves Signals Based Upon AR Model for Efficient Damage Inspection.

Syed Haider M. Rizvi[1*], and Muntazir Abbas[1,2]

[1]Corresponding author, department of Engineering Sciences, PN Engineering College, National University of Science & Technology, Pakistan

[2]SWEE, Cranfield University, College Road, Cranfield, Bedfordshire, United Kingdom

E-mail: contacthaider.rizvi@gmail.com

Abstract

The generation and acquisition of the ultrasonic guided wave in metallic or composite structures to investigate the structural defects are quite straightforward; however, the interpretation and evaluation of the reflected/transmitted signal to extract the useful information is a challenging task. It is primarily due to the dispersion, and multi-modal behaviour of the Lamb waves which is dependent on the exciting wave frequency and thickness of the material under investigation. These multi-modes and dispersion behaviour lead to a complex waveform structure, and therefore, require an advanced signal processing technique to decipher the useful information in time and/or frequency domain. For this purpose, Wigner-Ville Distribution, due to its desirable mathematical properties, is considered as a powerful tool for generating time-frequency spectrum and estimating temporal and spectral features of this type of complex signals. However, because of its quadratic nature, the undesirable cross-terms and spurious energies are also generated, which limit the readability and the interpretation of the spectrum. To suppress this effect, the autoregressive model based upon Burg's Maximum Entropy method was employed in the paper to modify the kernels of the discrete Wigner-Ville Distribution. This technique was applied to ultrasonic Lamb wave signals obtained numerically and experimentally under the different configuration to extract useful discriminating spectral and temporal information that was required for mode identification, structural damage localization, and its quantification. For damage localization, based upon excellent time-frequency energy distribution, the proposed method precisely estimated the distance between two closely spaced notches in a metallic plate from different simulated noisy signals with a maximum uncertainty of 5%. Moreover, the energy concentration of the time-frequency energy distribution in a combination with variation of its instantaneous frequency curve was also effective in identifying the overlapping modes of the Lamb wave signal. Lastly, for damage quantification, three time-frequency based damage indices namely, energy concentration, time-frequency flux, and instantaneous frequency were extracted from the five sets of specimens using the proposed time-frequency scheme and trained them for the regression model. The model testing proved that the damage indices have the potential to predict the crack sizes precisely and reliably.

Keywords: Lamb waves, signal processing, time-frequency analysis, Wigner-Ville distribution, autoregressive model, maximum entropy method, Non-destructive testing,

1. Introduction:

Damage identification techniques in metallic or composite structures based upon the generation and acquisition of the Guided Ultrasonic Waves (GUW) have been widely acknowledged as an effective tool for Non-Destructive Testing and Evaluation (NDT&E) [1–4]. These waves have advantages of long-distance propagation and hence can be used to inspect the large area with minimum equipment installation [5]. The accuracy and precision of this approach are largely dependent on the processing and interpretation of the signal. When the guided wave such as Lamb wave is excited in a structure, the wave propagates and encounters

different interferences in its path, causing wave scattering. These scattered waves contain comprehensive information about the state-of-health of the structure [6]. However, they are extremely complicated to interpret and extract useful information as they contain multimode and exhibit dispersions [7]. Therefore, in order to extract useful information from such non-stationary complex signals, the use of an effective signal processing scheme is necessitated.

Several signal processing techniques have been developed to identify the wave features. A method, called Dispersion Compensation proposed by Wilcox [8] may be a possible solution. This technique is based upon the fact that the dispersion compensated signal can be acquired by tracing backward the recorded signal to its source. Fundamentally, this method fits best for single wave component, however recent works have advanced this method for multi-components [9]. This approach is limited by the requirement of theoretical information about dispersion curve of the structure and works best if the dispersion characteristics matches well with the actual one. Moreover, the compensated wave packet is deformed compared with original excitation [10].

Recent work in time-frequency signal processing have shown promising results. Aiming to overcome uncertainty principle in linear TFR and cross-terms in bilinear TFR, and to extract the maximum features of the signal, some improved TF techniques have been proposed. For example, linear TF method such as Chriplet transform (CT) and wavelet transform (WT), have been developed for the analysis of multicomponent lamb wave signals. For example, Zhao [11] used Ploy Chriplet transform (PCT) along with time-varying Vold-Kalman filter to identify the different overlapped modes of the signal. However, the method requires prior knowledge of the dispersion curve of the structure. Similarly, Liu [12] used synchrosqueezed WT method to improve TFR resolution and identify mode energies in TF plane. It's a special case of post-processing reassignment technique which only reassigns the scale variable of WT into frequency variable. By doing so, the time resolution of the signal may be preserved. However, the reassignment method may still generate blurry TFDs for fast-varying overlapping signal components [13].

In case of bilinear TFD, Wigner-Ville distribution, a Cohen's class, offers best TF resolution while exhibiting least amount of spread in TF plane and satisfies a large number of desirable mathematical properties like reality, symmetry, marginality, time and frequency shift, etc. [14]. These desirable properties are attained with some limitations. For example, if a signal has multiple components; the negative energy levels or spurious energies and cross-terms (interferencse terms) which do not have any physical interpretation, may appear in the distribution [15,16]. Additionally, bilinear TF methods are also sensitive to the

signal-to-noise ratio (SNR) therefore, multiple components along with low SNR value may exacerbate the TF spectral resolution which severely affects the accuracy of the Lamb wave inspection [17]. In the literature, these cross-terms are mostly attenuated by exploiting the smooth operation. Designing the smooth kernel in a 2-D Fourier domain or filtering the definition by introducing a low-pass window function can significantly reduce the influence of the cross-terms. These are Smoothed-Pseudo Wigner-Ville Distribution (SPWVD) [18] or its reassigned version i.e. Reassigned Smooth-Pseudo Wigner-Ville Distribution (RSPWVD) [19], Choi-William Distribution (CWD) [20,21] and Cone-Shape Distribution (CSD) [22]. However, all these methods have limitations [23] and cannot be implemented in all types of complex signals [7]. For example, smoothing in SPWVD causes auto-terms to be smeared and as a result, the distribution reduces its concentration [23]. On the other hand, the efficiency of the CWD and CSD are highly dependent on the nature of the analysed signal; If some components of the signal are synchronized in time, both CWD and CSD will present strong interference [24].

The Maximum Entropy (ME) method developed by Burg [25] has been widely used for the spectral analysis. Recently, Zoukaneri [26] and Wang [27] have exploited ME algorithm based upon the Autoregressive (AR) model for the calculation of high-resolution Wigner-Ville TF distribution for low-frequency seismic applications. Zoukaneri [26] used conventional Burg's Maximum Entropy Spectral Analysis (MESA) algorithm to compute the coefficients of the AR model/ prediction error operator (PEO) for each discrete Wigner-Ville kernel sequences. The application of MESA is, however, limited to the standard autocorrelation sequences and does not work for Wigner-Ville; which is categorized in instantaneous autocorrelation sequences [27]. Instead of the conventional Burg ME algorithm, Wang [27] used Andreson ME algorithm [28] in the Multichannel fashion in which the average of the multiple kernel sequences was used to determine the coefficients of the AR model/ PEO. In this paper, we use a segment-based ME method for the multi-modal ultrasonic lamb waves signals. For this purpose, first, the discrete Wigner-Ville Kernel sequences are calculated by exploiting the instantaneous autocorrelation sequence of infinite lag, and then a short window is assigned to a part of the kernel sequences where there is no cross-terms present. Here, these kernel sequences would serve as several separate segments of the missing data and, therefore, Wael and Broersen [29] Burg algorithm for segments is employed to compute the reflection coefficients. The conventional Burg algorithm determines the reflection coefficient by minimizing the backward and forward prediction error of a single sequence or segment. Whereas Wael and Broersen algorithm

is highly efficient in estimating the prediction error of all the segments taken together and hence a single model can be exploited for all the kernel sequences at a time. This model is more robust, stable, less biased, and computationally efficient that generates minimum phase PEO. These operators are then exploited to generate high resolution time-frequency distribution. The main contributions of the work are: (1) an improved segment based ME algorithm is employed to improve the kernels of WVD by using segment based ME method, (2) the proposed scheme is then employed for Lamb wave modes identification and structural damage localization, (3) Three time-frequency based damage indices are calculated by the proposed method to quantify the structural damage.

The remainder of this paper is organized as follows: The first section explains the theoretical background of the Time-Frequency (TF) signal processing techniques and their general limitations. While in the second section, the methodology and proposed ME algorithm is derived and discussed at length. In the third section, Lamb wave signals obtained under different configurations are exploited to verify the credibility and effectiveness of the proposed method. The conclusions are outlined in the last section.

2. Theoretical Background:

2.1 Time-Frequency Analyses and Their General Limitation:

A time-domain representation or its Fourier spectrum does not provide adequate information about the frequencies of the signal generated as a function of time. Separate analysis (either in time or frequency domain) compromises the information available in the other dimension of the signal. The logical resolve is to represent the signal or distribution whose domain in both dimensional spaces (t, f). Such type of distribution is called the Time-Frequency Distribution (TFD) [6].

The basic objective of the TFD is to represent the energy density of the signal in both time and frequency. However linear TFD suffers from the Heisenberg Uncertainty Principal making it almost impossible to simultaneously generate a spectrogram that has a perfect resolution in both time and frequency [7]. The Linear TFD e.g. Short-Time Fourier Transform (STFT), Chriplet Transform (CT) or Wavelet Transform (WT) are based on the Fourier Transform using linear superposition principle that weighs the density of the signal by decomposing the signal into the time and frequency domain. This method achieves the signal localization in the time domain by dividing the signal into a series of small overlapping segments called window and then the Fourier Transformed (FT) is applied to each segment. Each FT provides a frequency domain information associated with the time value at the window centre. STFT uses fixed window function while CT and WT performs this operation by a flexible and time-varying window. However, the obtained resolution of the spectrograms by these methods entirely depends upon the type of the window and its size. A wide window function provides good frequency resolution but worsens the time resolution. Similarly, the vice-versa in case of a narrow window and hence generates smearing of temporal and/or spectral information [30]. On the other hand, the bilinear or quadratic TFD, where the signal enters twice in its calculation e.g. Wigner-Ville Distribution (WVD), is not constrained by this uncertainty principle [31] as it does not require any window functions and therefore WVD has the characteristic of the perfect resolution, time-frequency edges, and energy concentration. Moreover, unlike the linear TF distribution which can only express the approximate energy distribution in TF domain, WVD can well represent the true TF energy distribution of the signal [32]. However, being quadratic in nature, the accuracy of the WVD seriously suffers from the inherent cross/interference terms when a signal contains multiple components and high noises [33].

2.2 Wigner-Ville Distribution and Cross Terms:

The Winger distribution, at any given instant of time, is the FT of the instantaneous autocorrelation sequence (kernel) of the infinite lag [14]. The Wigner distribution in terms of the analytical signal z(t) of the raw signal s(t) is called the Winger-Ville Distribution (WVD), which is,

$$W_z(t, \omega) = \int_{-\infty}^{+\infty} z\left(t + \frac{\tau}{2}\right) z^*\left(t + \frac{\tau}{2}\right) e^{-i\omega\tau} d\tau \quad (1)$$

Now if the signal s(t) contains two mono-components

$$s(t) = s_1(t) + s_2(t)$$

Equation 1 will become,

$$W_{12}(t, \omega) = W_{11}(t, \omega) + W_{22}(t, \omega) \\ + W_{12}(t, \omega) + W_{21}(t, \omega)$$

Since $W_{12}(t, \omega)$ and $W_{21}(t, \omega)$ are the complex conjugate of each other i.e. $W_{12}(t, \omega) = W_{22}^*(t, \omega)$ therefore,

$$W_{12}(t, \omega) = W_{11}(t, \omega) + W_{22}(t, \omega) \quad (2) \\ + 2Re\{W_{12}(t, \omega)\}$$

Unlike the linear TFD, the WVD of the signal containing two mono-components is the sum of WVD of each component, called the auto-term, $W_{11}(t, \omega)$ & $W_{22}(t, \omega)$, in

equation 2, and has an additional term, $2Re\{W_{12}(t,\omega)\}$, which is the cross-term or interference term. If a multi-component signal has *n* components, then *n(n-1)/2* cross-terms will generate in the distribution [34]. These cross-terms are oscillatory in nature and exist between the auto-terms which give rise to an artifact and give false impressions about the distribution. Therefore, cross-terms in bilinear TFD cause serious problems in interpreting the distribution especially if the signal contains numerous components and noises [35].

3. Methodology:

In this paper, the cross terms in WVD were suppressed by Burg's ME method proposed by Zoukaneri and Porsani [26]. The intuition of this method is to modify the discrete WV kernels by extending its sequence from the part without cross-terms to the outside of this part. This method computes the minimum phase prediction error operators (PEO) using Burg's ME algorithm for segments which are then used to estimate the coefficients of the extended discrete WVD kernel sequences and provides high-resolution Time-Frequency spectrum.

3.1 Discrete Wigner-Ville Distribution (DWVD)

First, in order to avoid the spectral aliasing, the signal x(n) is sampled at the twice the normal Nyquist rate and then calculate the analytical signal z(n) by using Hilbert Transform (HT) which is,

$$z(n) = x(n) + JH[x(n)]$$

Where n is the time sample index, H[x(n)] is HT of the signal x(n). Now in equation 1 if $t = nT_s$, and $\tau = 2lT_s$, the Wigner-Ville kernels can be discretized as,

$$K^{(l)} = Z(n+l)Z^*(n-l)$$

Where the power of K indicates the indices of the kernel. $l = \{-L, \dots -1, 0, 1, \dots, L\}$; $K(0) = Z(n).Z(n)$. Moreover, due to conjugate symmetry of the kernels, $K(-l) = K(l)$.

The Fourier Transform of these kernels generates discrete Wigner-Ville distribution.

$$W^{(m)} = \sum_{-(N-1)/2}^{(N-1)/2} K^{(l)} W_4^{ml} \tag{3}$$

Because here the DWVD has the periodicity of (N-1), the frequency interval of the above equation is half of the frequency interval of the standard discrete FT. Therefore,

additional power 2 represents the scaling factor, is appearing in the twiddle factor.

3.2 Maximum Entropy Wigner-Ville Distribution (ME-WVD)

The general equation of Burg's Maximum entropy spectrum is given as,

$$P(f) = \frac{P_m}{B\left|1 + \sum_{i=1}^{J} \alpha_i e^{-j2\pi f iT}\right|^2} \tag{4}$$

Where P is the final prediction error; B is the signal Bandwidth corresponding to the signal period of $T = 1/2B$. The equation indicates that the Maximum Entropy spectrum is similar to that of the Autoregressive model with coefficient α_i [36]. The Burg method directly estimates the reflection coefficient R_α and then uses the Levinson recursion algorithm to estimate the Prediction Error Operator (PEO) or Prediction Error Filter (PEF). The reflection coefficients R_α are estimated by minimizing the average energy of forward and backward prediction error while satisfying the Levinson Durbin recursion.

A forward and backward linear prediction with PEO α_j of segment *S* can be given as,

$$\widehat{K_S^{(l)}} = -\sum_{i=1}^{J} \alpha_{[J]}^{(i)} K_S^{(l-i)}$$

$$\widehat{K_S^{(l)}} = -\sum_{i=1}^{J} \alpha_{[J]}^{*(i)} K_S^{(l+i)}$$

Where J is the prediction order. The residual between the actual and the predicted kernel is known as the prediction error $e^{(l)}$ which is,

$$e^{(l)} = K_S^{(l)} - \widehat{K_S^{(l)}}$$

Similarly, the forward and the backward residual can be calculated by

$$f_{S[J]}^{(l)} = K_S^{(l)} - \left[-\sum_{i=1}^{J} \alpha_{[J]}^{(i)} K_S^{(l-i)}\right]$$

$$b_{S[J]}^{(l)} = K_S^{(l)} - \left[-\sum_{i=1}^{J} \alpha_{[J]}^{*(i)} K_S^{(l-i)}\right]$$

If R_J is the reflection coefficient then the forward and backward prediction error can also be written as,

$$f_{S[J]}^{(l)} = f_{S[J-1]}^{(l)} + R_{[J]}b_{S[J]}^{(l-J)}$$

$$b_{S[J]}^{(l)} = b_{S[J-1]}^{(l)} + R_{[J]}^{*}f_{S[J]}^{(l+J)}$$

Note the average estimated prediction error energy is given as,

$$E_{[J]} = \frac{1}{2}\sum_{S}\left(\sum_{l=J}^{N}\left|f_{S[J]}^{(l)}\right|^{2} + \sum_{l=0}^{N-J}\left|b_{S[J]}^{(l)}\right|^{2}\right) \quad (5)$$

Since in each iteration the number of residual decreases i.e. the size of the vector of the backward and forward residual between the two consecutive steps would not have the same length, therefore for the convenience, we use f' and b' for the residuals of previous steps.

$$f_{S[J]} = f'_{S[J]} + R_{[J]}\,b'_{S[J]}$$

$$b_{S[J]} = b'_{S[J]} + R_{[J]}^{*}f'_{S[J]}$$

For the minimum phase prediction error filter and to make the condition for the filter to be stable, the average error energy must be minimum. Therefore, by taking $\partial E_{[J]}\big/\partial R_{[J]} = 0$ in equation 5, a general equation for the reflection coefficients can be deduced as,

$$R_{J} = \frac{-2\sum_{s}\langle f'_{S[J]},\, b'_{S[J]}\rangle}{\sum_{S}\left(\left\|f'_{S[J]}\right\|^{2} + \left\|b'_{S[J]}\right\|^{2}\right)} \quad (6)$$

Where $<.>$ denote the inner product and $\|.\|$ shows the induce norm i.e. $\|x\| = \sqrt{\langle x, x\rangle}$

The above equation shows that all the $|R_{J}| \leq 1$ that proves the stability and generates minimum phase PEO which can be estimated by the Levinson-Durbin algorithm.

$$\alpha_{J}^{(i)} = \alpha_{J-1}^{(i)} + R_{J}\alpha_{J-1}^{*}{}^{(J-i)},\; i = 0,1,\dots,J$$

In the above equation, $\alpha_{J}^{(0)} = 0$ and $\alpha_{J}^{(J)} = R_{J}$ Therefore, J^th prediction order generates (J+1)^th PEO.

The number of kernels appears at the front part of the sequence, which is supposed to have no cross-terms [27], are used to predict the other kernels sequence outside of this free-interference window. The size of this window, let say W, controls the spectral resolution of the distribution. To get the spectrum sharper with reasonable accuracy, the size of W

should be small and finer [26]. Mostly, for the ultrasonic Lamb wave signals, the window size is usually between 5% and 7% of the total number of kernels in a segment which is enough to generate a high-resolution spectrum. However, the range may be greater depending upon the nature of the signal. For example, if the signal has a very low SNR value, the range must be higher. Moreover, due to the conjugate symmetry of the kernel i.e. $K(l) = K(-l)$, only half of the kernel sequence will be considered for the modification of Wigner-Ville Kernel sequences.

To compute the extended kernel, the forward prediction is,

$$K^{(W+n)} = -\sum_{i=1}^{N}\alpha_{[J]}K_{S}^{(W+n-i)}$$

After applying the conjugate symmetry of the kernels, the DFT is performed on the predicted kernel to obtain the maximum entropy WVD.

$$W^{(m)} = \sum_{-(N-1)/2}^{(N-1)/2}K^{(l)}W_{4}^{ml} \quad (7)$$

3.3 AR Model Estimation

The Burg method ensures a stable AR model, but its accuracy is highly dependent upon its order. Therefore, a perfect order that is used to describe the given data, is essential for generating high-resolution TF spectrum. This can be estimated by selecting appropriate information criterion. In this study we use the Akaike Information Criterion (AIC) for multiple segments of length N is

$$AIC = \ln\big(Res(J)\big) + \frac{2J}{SN} \quad (8)$$

Where,

$$Res(J) = \delta^{2}\prod_{i=1}^{J}(1 - R_{i}^{2})$$

In the above equation, δ^{2} is the residual variance for a fitted AR(J) model. The best model is the one with minimum AIC value. Our experience indicates that for the Lamb wave signal, the model order greater than 5 does not put any significant effect on the accuracy of the AR model. Therefore, the order within the range of 5 is enough to ensure the high resolution
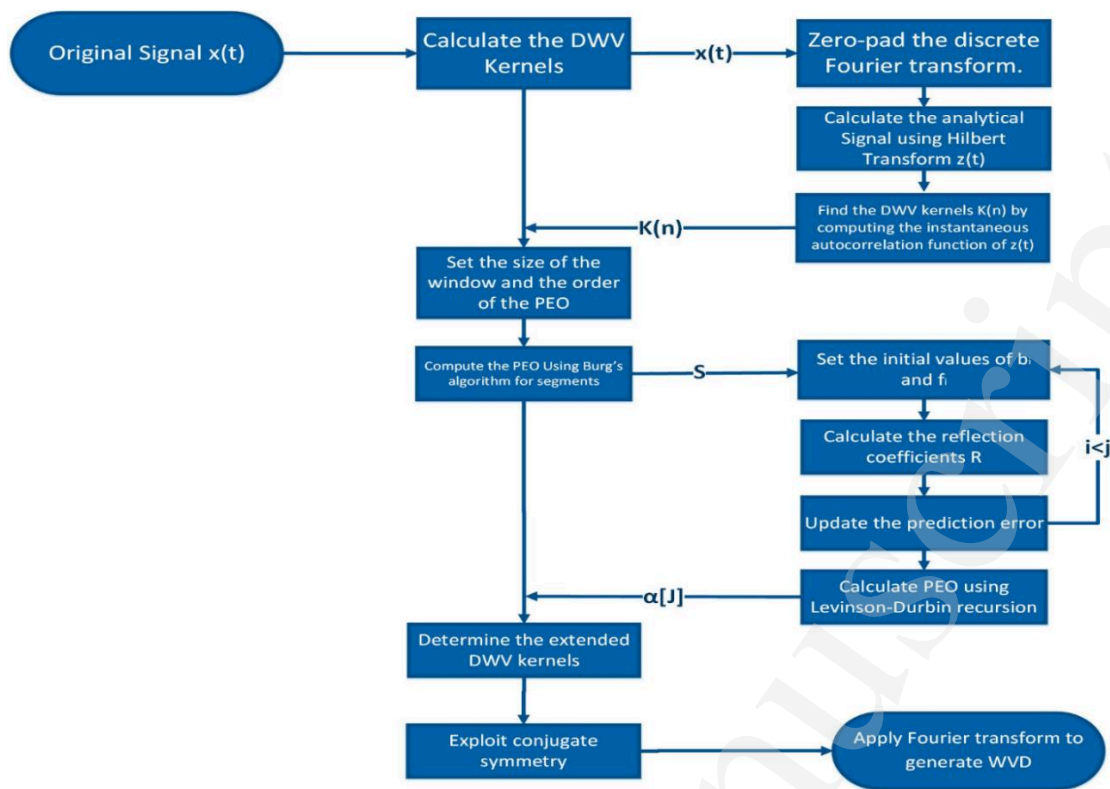
Figure 1: Steps of computing Wigner-Ville Distribution with Maximum Entropy Method

of the distribution. Figure 1 summarizes the steps of the ME-WVD algorithm, used in this study.

4. Numerical Investigation of Proposed Method:

4.1 Synthetic Chirp Signals:

First in order to check the concentration of the TFD generated by the different TF method, intersecting concave and convex chirps were sampled at 1kHz for 4 sec. The instantaneous frequencies of each chirp are given by figure 2.

Figure 3 shows that the proposed method significantly reduces the cross-term effect, maintains the sharpness of the spectrum with the small spread on time-frequency plane. On the other hand, PCT has better resolution but high spread on time-frequency plane. SPWVD and CWD are blurred and difficult to interpret while RSPWVD and CSD generate sharp and high-resolution distribution but their performance deteriorated due to the presence of discontinuities.

Moreover, to quantify the concentration of the TFD, the most promising approach based upon the entropy function has been exploited. Peaky and concentrated TFDs would generate small entropy values [37]. In this paper Rényi entropy, normalized with distribution volume is utilized to measure the distribution concentration. Which is given by equation 9. Normalized Rényi entropy detect the zero mean cross terms and therefore if the signal contains oscillatory cross terms, then the high
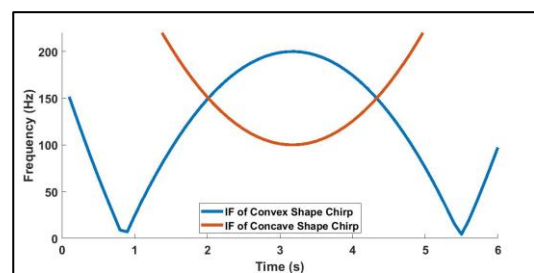
entropy value would be generated which indicates low concentration.

$$RV_{norm} = -\frac{1}{2}log_2\left(\sum_T \sum_F \left(\frac{W^3(T,F)}{\sum_T \sum_F(|W(T,F)|)}\right)\right) \quad (9)$$

Figure 4 represents that RSPWVD generates the smallest entropy while MEM, PCT and CSD estimate comparatively similar entropy values but slightly larger than RSPWVD which means that these methods generate peaky and highly concentrated TFD. However, there are some shortcomings in visual inspection of PCT, CSD and RSPWVD method which has already been discussed.

From the next section, we shall apply the proposed method to guided wave signals obtained numerically and experimentally to extract useful discriminating spectral and temporal information that is required for mode identification, structural damage localization, and its quantification.

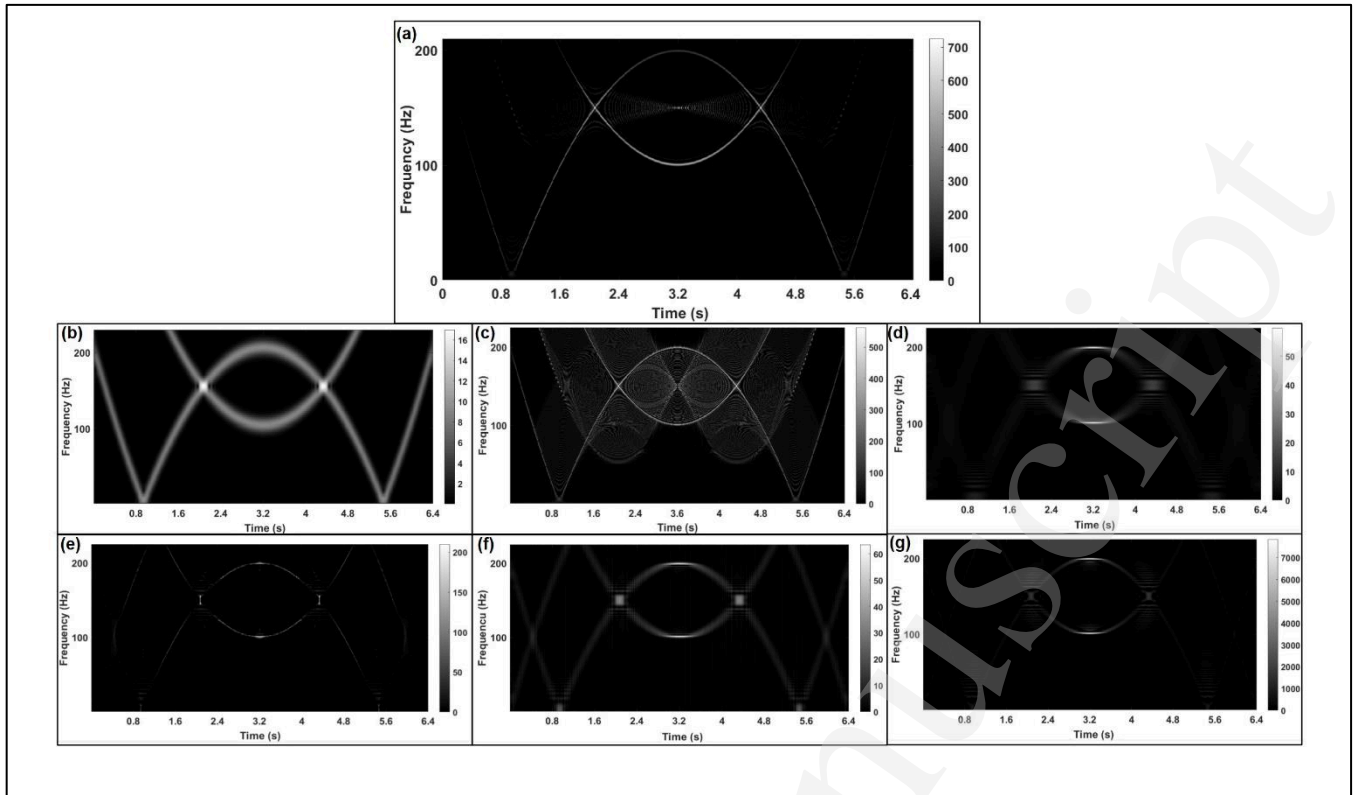**Figure 2:** Instantaneous frequency of two intersecting chirp

Figure 3: Time-frequency domain energy distribution: (a) proposed ME-WVD; (b) PCT; (c) WVD; (d) SPWVD (Kaiser Window, g = N/10, h = N/4); (e) RSPWVD; (f) CWT (δ = 0.25) and (g) CSD.

4.2 Damage Localization:

Simulation for generation and acquisition of Lamb wave signals was done by using the commercial software Abaqus/Explicit® finite-difference module. Due to the computational limitation, the Multiphysics approach had not been utilized, therefore a specific modelling technique for PZT actuator and sensor was used, introduced in [38]. The convergence of the numerical results depends upon the temporal and spatial resolution of the finite element model [39]. The high time step results in high-frequency components that could not be resolved accurately. Hence to avoid the numerical instability, Moser [40] recommended that the integration time step must be small that there are minimum 20 times steps during each cycle of the wave at the maximum frequency to keep the explicit algorithm stable i.e. $\delta t < 1/20 f_{max}$. In this study, 2MHz frequency was used to generate the desired mode of the Lamb wave, therefore, δt was set to be 1.0×10^{-9} which satisfied the general requirement. Moreover, mesh density is also an essential factor. Moser [40] suggested that for a good spatial resolution at least 10 elements must be allocated in the shortest wavelength of the wave. The group velocity of the fundamental symmetric S_0 mode at this frequency is approximately 5243m/s which makes the wavelength of about 2.6mm. Therefore, the element size was set to be 0.20mm. It ensured that there were more than ten nodes across the shortest wavelength.

For the pulse echo-configuration, a two-dimensional FEM model in which four-node plane strain elements with encastre boundary condition was employed for an aluminium plate. The thickness of the plate was 0.4mm and its nominal properties are given in Table 1. The plate contained two adjacent notches of same the dimensions as shown in figure5. Different simulated results were obtained by changing the distance d between two adjacent notches (3.5, 4, 5, 6, and 7mm). The depth of each notch was 0.2mm. The excitation signal of the five-cycle wave pulse, which was modulated by Gaussian function, was applied parallel on the upper and lower surfaces of the plate.
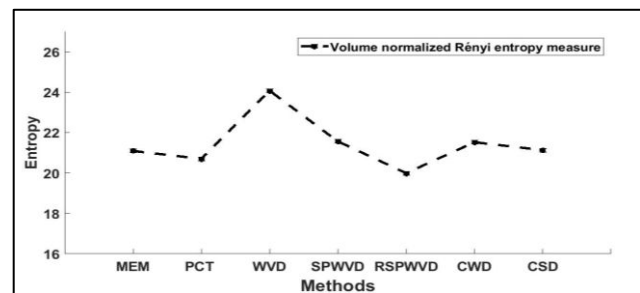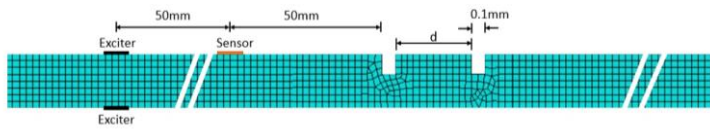

Figure 4: Value of criterion (Entropy) vs TFR methods.

Table 1: Nominal properties of the aluminum plate (6061-T6).

Young's Modulus, E (GPa)	Poisson's ratio, N	Density, P (kg/m³)	Yield Stress, Y (MPa)
72.4	0.33	2780	276 MPa

Figure 5: Two-dimensional numerical model with two notches.

Due to in-plane stresses, the symmetric mode S_0 was the dominant signal. The wave propagated and upon the interaction with the notches, some part of the wave energy reflected from the notches along with the reverberating echoes [41]. The two notches are very closed to each other; therefore, the reflected waves will overlap, making it more difficult to determine the position and gap between the notches from the measured signal precisely. Moreover, artificial noises were also added to original signals to check the noise robustness of the proposed method. The reflected signals from the notches are presented in figure 6.

The kernels of DWVD were stored in 4000 × 4000 matrix. In order to compute the prediction error coefficient α_i for S = 4000 samples, the optimum order of the PEO was found to be J = 4. figure 7 represents the contour plot of time-frequency distributions along with energy distribution in the time domain (instantaneous amplitude) of the given signal using the proposed ME-WVD, PCT, WVD, SPWVD, RSPWVD, CWD, and CSD when the distance between the notches was 4mm. As compared with the other methods, ME-WVD generated a sharp TF spectrum and two echoes can easily be observed by the energy distribution in the time domain. Theoretically, the wave velocity of the S_0 mode is equal to 5243m/s. The arrival time of the echoes computed by the different TF methods is exhibited in Table 2. The proposed ME-WVD based method worked much better and localized structural damages more precisely, whereas in all the other methods, smoothing significantly shift the auto-terms from their original location in the time-frequency domain and thus generate errors. Therefore, the results obtained by these kernel-based methods are rather unreliable. Similar results were obtained for different values of d, and maximum error in the estimation of the separation gap by the ME-WVD method were not more than 5% which is shown in figure 8. The main source of this error is attributed

to the fact that the scattered waves coming from the notches would experience dispersion.

5. Experimental Investigation of Proposed Method:

5.1 Wave Mode Identification:

To generate the different modes of the Lamb wave, experiment, based on pitch-catch configuration, were performed to generate the lamb waves in an aluminium plate alloy 6061-T6. The nominal properties of the alloy were the same as used in the numerical analysis. This aluminium alloy has a wide range of industrial application and most commonly used in the manufacturing of aerospace and automotive components such as wings and chassis. For experimental measurement, two small radials Piezoelectric Wafer Active Sensor (PWAS), 10mm diameter, and 1mm thickness with a silver electrode on both sides were used. The rigid bond between the PWAS and plate was done by using cyanoacrylate adhesive. A rectangular notch of dimensions 40mm×2mm×0.8mm etched through a pantograph machine was placed between the actuator and the sensor. A five-cycle Gaussian modulated sine wave signal with a central frequency of 200kHz was computed through Matlab®. At this configuration, S_0 mode would activate with larger amplitude than A_0. When these modes pass through damage, mode conversion phenomenon would be observed, breaking down the symmetrical nature of the signal, and extra waves would generate simultaneously.
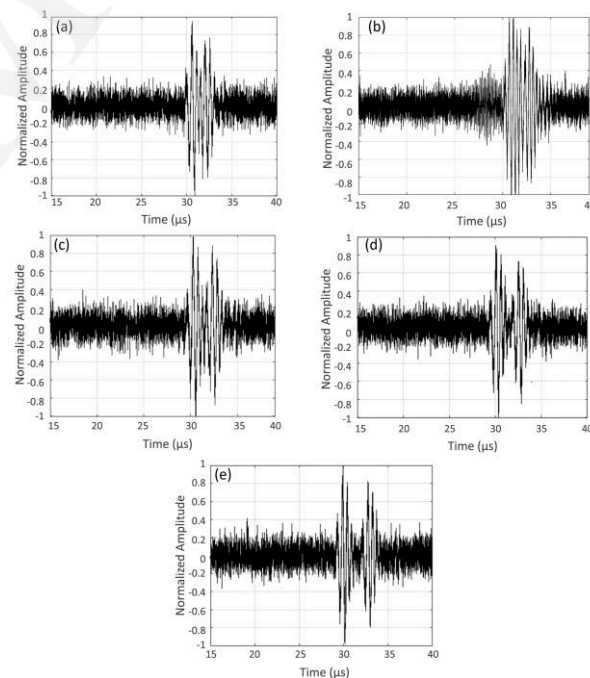

Figure 6: Reflected simulated signals from the two notches separated by: (a) 3.5mm; (b) 4mm; (c) 5mm; (d) 6mm; (e) 7mm. The signal-to-noise ratio (SNR) of all signal = 5 dB.

Table 2: Measurements of the arrival time of the echoes for the localization of two adjacent notches based on different TF.

TF methods	Arrival time of first echo (µs)	Arrival time of second echo (µs)	Distance between the notches (mm)	Percentage error
ME-WVD	31.107	32.664	4.1	2.5
PCT	31.098	32.787	4.4	10.0
WVD	31.684	32.901	3.2	20.0
SPWVD	31.188	32.538	3.5	12.5
RSPWVD	31.216	32.678	3.8	5.0
CWD	31.212	32.604	3.6	10.0
CSD	31.248	32.597	3.5	11.2
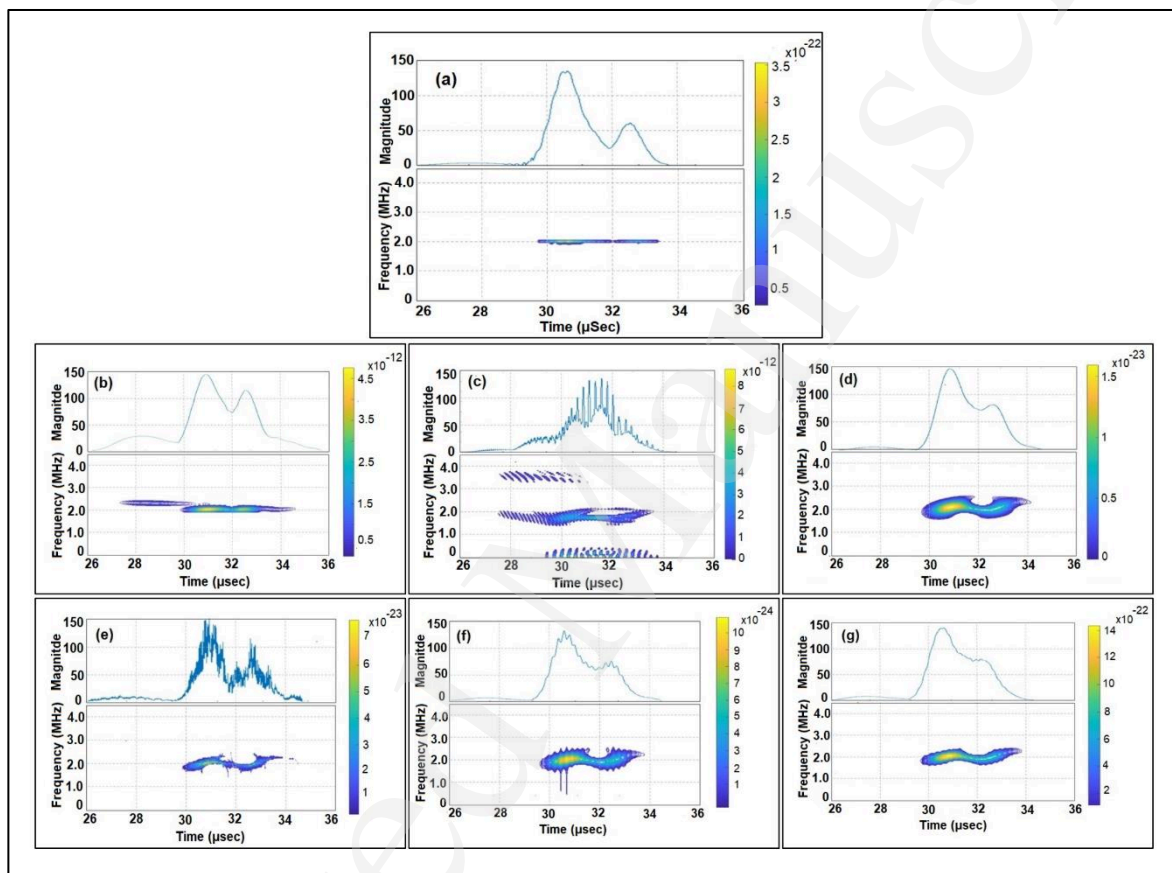
Figure 7: Contour plot and time-domain energy distribution for pulse-echo configuration (d = 4mm): (a) proposed ME-WVD; (b) PCT; (c) WVD; (d) SPWVD (Kaiser Window, g = N/10, h = N/4); (e) RSPWVD; (f) CWT (δ = 0.25) and (g) CSD.

The distance between the actuator and the sensor was 150mm while the crack was etched exactly at the centre i.e. 75mm. The complete experimental setup is represented in figure 9. The original damage signal along with its pristine signal received at the sensor is presented in figure 10. It can be observed that newly generated A_0., due to damage, is present between the actuating S_0 and A_0 mode, and due to the dispersion and the time-delay, the last two modes and overlapped with each other. This makes the extraction of different wave energy content and identification of different modes from the signal more difficult.

The sampling rate of the signal was 25MHz which generated 4001 samples within the given time range. To compute the prediction error operator α_i for the ME method, the optimum order was found to be J = 2. The time-frequency energy distribution obtained by the proposed method and other TF methods are given in figure11. The proposed ME method significantly reduced the spurious

energies and interference terms between the components of the signal such that the incident S_0, reflected A_0' from damage, and incident A_0 modes are clearly observed in ME-WVD by suppressing the cross-terms and its spurious energies, enhancing energy spots and non-stationary tendencies. PCT also separated the signal components but their localization become coarser due to increase of TF spread of the component. Similarly, the bilinear TFA in figure 11(d)-11(g), the smoothing failed to resolve the modes of the lamb wave signals composed by synchronized components that occur at the same time or the same frequency.
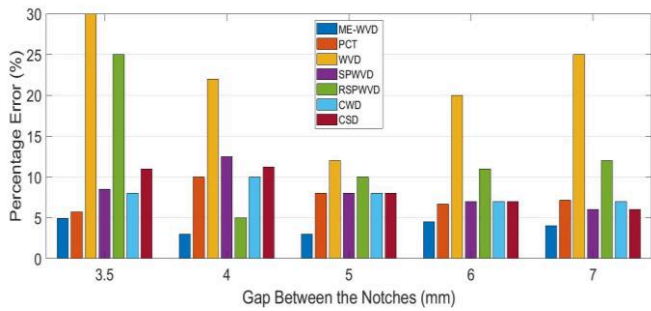

Figure 8: Percentage error when computing the gap between the notches by different TF methods.

Figure 9: Experimental Setup for wave generation using pitch-catch configuration.

Instantaneous frequency (IF), one of the important signal parameters obtained directly from the time-frequency distribution, provides essential information about the time varying spectral changes in a non-stationary signal and hence may be used for the mode identification. The robust and stable IF can be generated from the time-frequency distribution by estimating the first moment of WVD. This can be expressed as,

$$f(t) = \frac{\int_{-\infty}^{+\infty} f W_{MEM}(t,f)}{\int_{-\infty}^{+\infty} W_{MEM}(t,f)} \qquad (9)$$

In figure 12, IF and instantaneous amplitude (IP) of the underlying signal are compared with its baseline (undamaged) signal. In the figure, different trajectories are clearly shown in

the IF curves of the damaged signal corresponding to their envelops in IP. The highlighted trajectory represents the reflection from the crack. Similar trend is also observed in the signal received from the smaller crack size (10mm) of a different specimen, presented in figure 13, along with its IM and IF curves. The signal contains actuating S_0, and A_0, reflected A_0' from the crack, and S_0 reflections from boundaries. However, due to severe modes interference and overlapping, they cannot be straightforwardly distinguished from simple time-domain signal, figure 13(a). On the contrary, peaks in IF corresponding to its IA curve, clearly reveals the phase changes in the signal with respect to time. The arrival of different mode packets results in sudden variation in the IF curve. These variations are also noted at the end of each wave packets and hence a trajectory is formed. The length of these trajectories i.e. the distance between the wave-front and the trailing end in the IF curve can be used to estimate the wave travelled distance and velocity, and its time of arrival (ToA). Moreover, the information can be exploited to track the damage location if a network of transducers, offering multiple reflected or forward-scattering waves, is used [6]. It is also observed that the size of the trajectory formed by the forward-scattering waves increase with size of
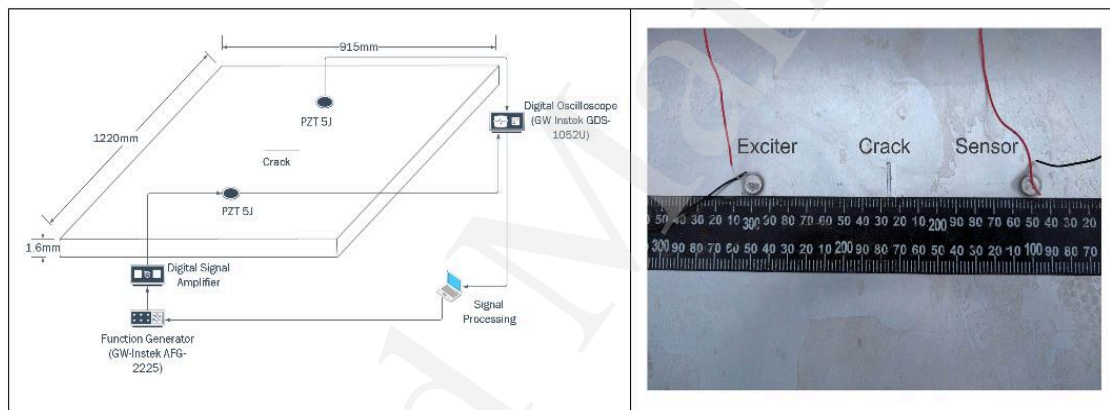
the crack. Moreover, greater crack sizes correspond to higher variations of phase pristine signal is taken as a reference, IF of the damage signal increases with the severity of the damage. This technique will be used to estimate the size of the damage in the next section.
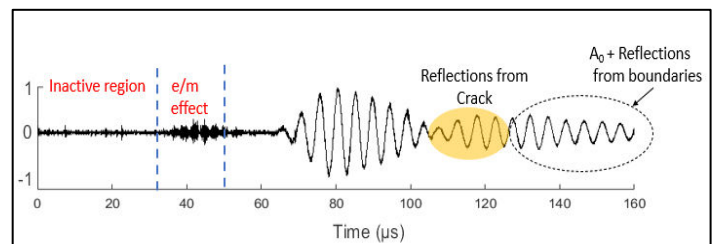

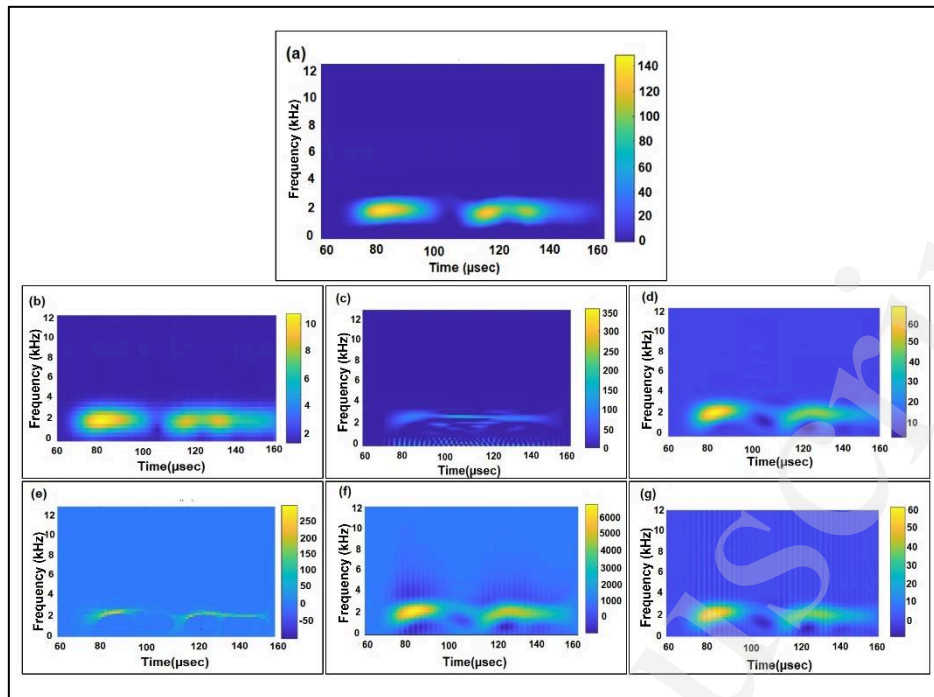**Figure 10:** Original waveform of the damaged Lamb wave.

Figure 11: Time-frequency domain energy distribution for damaged signal: (a) proposed ME-WVD; (b) PCT; (c) WVD; (d) SPWVD (Kaiser Window, g = N/10, h = N/4); (e) RSPWVD; (f) CWT (δ = 0.25) and (g) CSD.
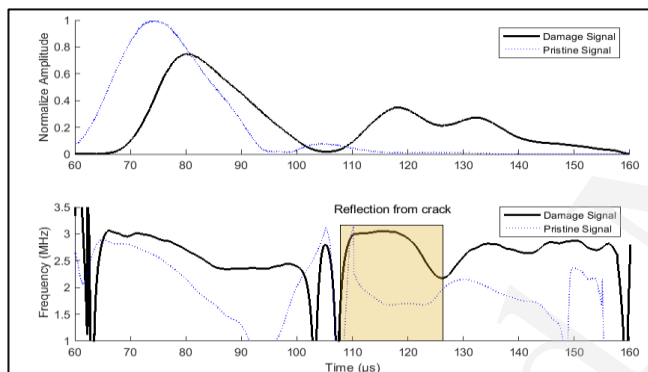

Figure 12: Instantaneous amplitude and instantaneous frequency of the damage and pristine signals.
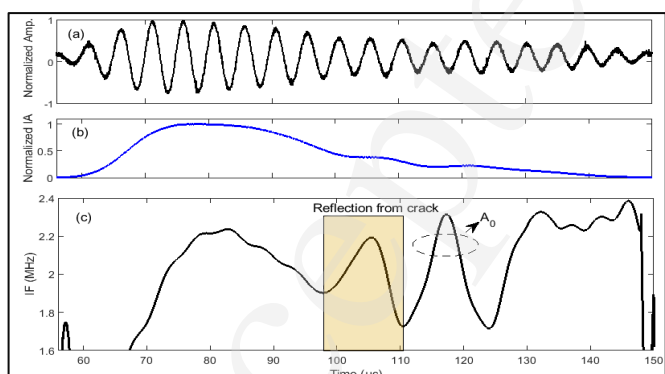

Figure 13: Instantaneous amplitude and instantaneous frequency of the damage signals: (a) original signal; (b) IA; (c) IF.

6 Crack Quantification:

In the previous sections, the proposed algorithm was successfully applied for damage identification and localization. To further extend this algorithm, the size of the damage will be estimated in this part which requires more information from the signal than damage location estimation[42].

6.1 Feature Extraction:

Damage feature extraction is the method of identifying the damage-modulated properties and parameters in a measured signal[6]. It is therefore an essential stage of an overall scheme for recognizing the pattern and classifying the abnormalities from the given signal for any regression tool or machine learning algorithm[43]. To characterize the damage, appropriate signal features must be selected with great care which are the most sensitive to variation in damage parameter. Traditionally, separate temporal, or spectral characteristics of a signal are used to estimate the damage indices for NDT applications. However, for the non-stationary signals i.e., a signal whose spectra change with time, these separate domain features may lack sufficient discriminating information about the underlying signal. TFD provides additional information about the non-stationary signal that cannot be directly obtained from the time or frequency domain. In this study, joint time-

Table 3: Experimental values of three damage indices estimated through the proposed time-frequency technique for S_1

Crack Length (mm)	Energy Concentration (EC) (10^9)	Normalized Amplitude (EC/EC*)	Time-Frequency Flux (TFF) (10^8)	Normalized Amplitude (TFF/TFF*)	Instantaneous Frequency (IF) (10^6)	IF Increment (IF/IF*)
0	13.2*	1.00	7.73*	1.00	3.0726*	1.00
5	10.3	0.7812	5.83	0.7535	3.0814	1.0028
10	7.42	0.5621	3.92	0.5071	3.0902	1.0057
15	6.94	0.5257	3.51	0.4541	3.1350	1.0203
20	6.54	0.4889	3.10	0.4011	3.1838	1.0362
30	5.48	0.4155	2.28	0.2949	3.2774	1.0667
40	4.51	0.3422	1.46	0.1889	3.3710	1.0971
50	4.17	0.3158	1.40	0.1815	3.5216	1.1461
60	3.82	0.2894	1.35	0.1742	3.6721	1.1951
70	3.47	0.2631	1.29	0.1668	3.8227	1.2441
(Asterisk) = pristine signal values (first row)						

frequency (t, f) based damage indices were used to estimate the variation of the signals to quantify crack size. These are,

☐ Energy concentration (EC); it represents the energy distribution over the time-frequency plane. Its mathematical expression is given in equation 10.

$$EC = \left(\sum_{t=1}^{T} \sum_{f=1}^{F} |W_{MEM}(t,f)| \right)^2 \qquad (10)$$

☐ Time-Frequency Flux (TFF); It is the rate of change of energy content of a signal in time-frequency plane. It is expressed as,

$$TFF = \sum_{t=1}^{T-l} \sum_{f=1}^{F-q} |W_{MEM}(t + l, f + q) - W_{MEM}(t,f)| \qquad (11)$$

Where l and k are the predefined values correlated with the rate of change of the signal energy which can be any integer value from 0 to T-1 and 0 to F-1. In this study, we used l = 1 and q=1 to estimate TFF. It can estimate small variations in energy of the signal which takes place either in time or spectral axis[35]

☐ Instantaneous frequency (IF); It accounts for the spectral variation of a signal as a function of time. Its general expression is given in equation 9. Since IF is sensitive to noise and may generate ambiguous peaks if signals have low SNR values. Therefore, to avoid this undesirable effect and to make the results more precise, the typical time-domain signals having high-frequency electromagnetic noises were first filtered through the fourth order Butterworth low-pass filter. The proposed ME-WVD was then applied to the filtered signal and then using equation 9, IF curves were extracted in the time-frequency domain. It was

noted that when the wave passes through damage present in its path, its phase change (IF) varies with the size of the crack and increases with larger crack sizes.

6.2 Crack Size Quantification Model:

Different sets of specimens, made of 6061-T6 aluminium, with artificial cracks of varying lengths were used to obtain the required measurement data while the width and depth of the crack (2mm and 0.8mm respectively) were kept constant while the length of the crack varied depicting crack propagation. Moreover, the orientation of the cracks was perpendicular to the monitoring path. All the arrangements are the same as shown in figure 9. Table 3 presents the experimental values of the required features i.e., TFF, IF and EC versus crack lengths, obtained by pitch-catch configuration of the first set of specimens. The first row is the benchmark signal obtained from the undamaged plate. Some of their received signals are given in figure 14. The relation between these parameters and crack length of all the specimens are shown in figure 15. It can be observed that all damage sensitive features exhibit a linear relationship with
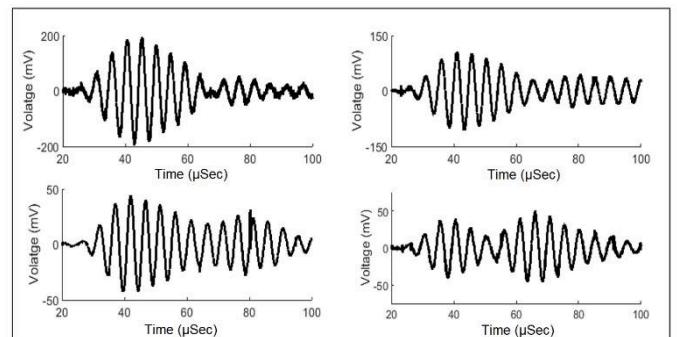

Figure 14: Received signals from the sensor for specimen S1 at different crack lengths: (a) pristine condition; (b) 10mm; (c) 40mm; and (d) 70mm.

crack size. EC and TFF both parameters decrease with the increase of crack length while peaks of IF increase with it. Moreover, it is also noted that each specimen has non-overlapping unique trends and follow different routes due to manufacturing and loading variabilities [44].

In order to establish the relationship between crack size and damage features, a linear regression model was trained using training data sets and evaluated using the validation sets in Matlab® regression learner app. In the first case, first four sets of specimens (S1, S2, S3, and S5) were used for training the model while S4 was used for testing while in the second case, (S1,S3, and S4) were exploited for training purpose and S3 and S5 for the model testing. Similarly, for the third case, training model sets were S1 and S2. Figure 16 compares the actual size of cracks and the model prediction of crack size. To further estimate the fitting performance of the model, median prediction, and 95% confidence interval are presented in the figure. It is observed that all the predicted values

proposed algorithm are found to be effective and generates satisfactory prediction results for the crack quantification.

In addition, the robustness and stability of the proposed time-frequency based regression model are further checked by predicting the values outside the horizon of the training size limit by using the extrapolation method. Extrapolation is usually not recommended for the machine learning regression model because the trends in the training data do not necessarily hold outside the scope of the model, therefore cannot be used for realistic models. However, here the main intuition is to check the stability and reliability of the damage indices and their correlation with damage sizes. For this purpose, maximum 100mm crack size specimens were used to estimate the values of the damage indices. The original signal received from the first specimen is presented in figure 17. Three damage indices i.e. EC, TFF and IF of all the 100mm crack size specimen are given in table 4. The first and the third specimen generate more reliable values with a maximum
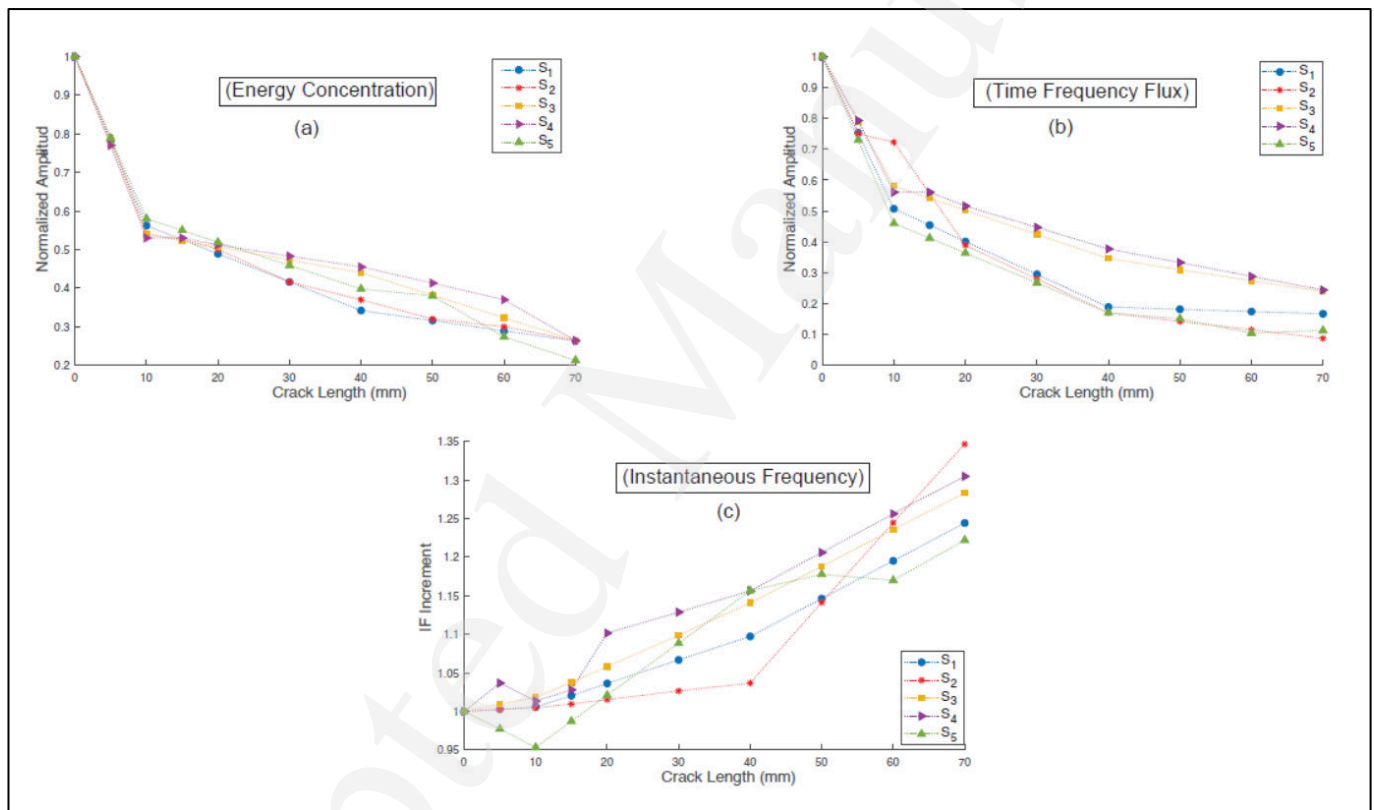

Figure 15: Crack size versus all three time-frequency based signal features for all five sets of specimens: (a) Energy concentration; (b) time-frequency flux; (c) Instantaneous frequency.

(squares) in figure 16(a) and (squares/triangles) in figure 16(b) follow the general trends of training data (circles) and the values are within the 95% confidence interval. A good agreement between actual and predicted measurements is observed. Moreover, prediction residue standard deviation for all cases were found to be 0.4891 and 0.4753 and 0.5257, respectively. Hence these damage features obtained by the

uncertainty of less than 3%. However, the second specimen gives some higher error value than expected which is <10%, mainly due to high manufacturing variabilities.

7. Conclusion:

In this paper, the autoregression model based upon Burg's maximum entropy method was employed to improve the
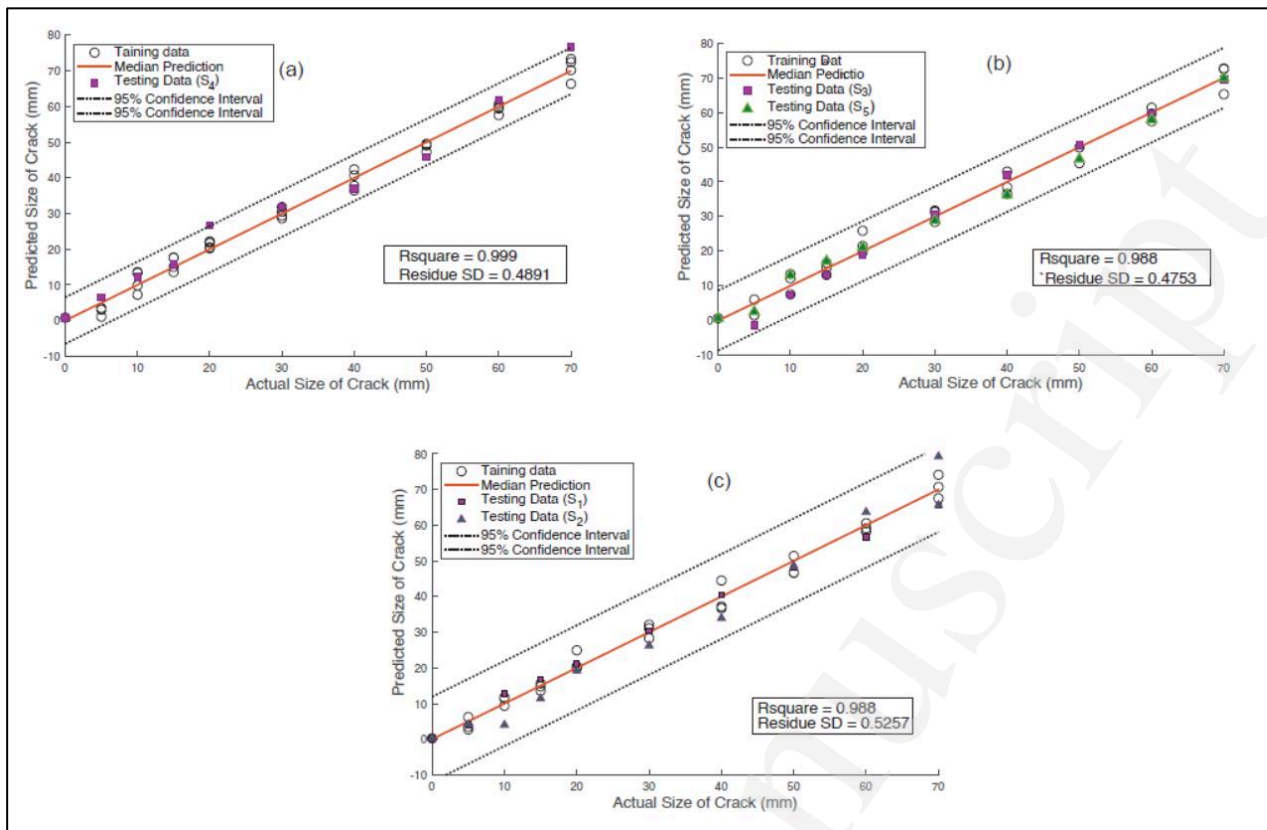
Figure 16: predicted size vs actual size of the crack using machine learning linear regression mode: (a) S4 testing data; (b) S3 and S5 testing data; (c) S1 and S2 testing data.

kernels of discrete Wigner Ville distribution which suppressed the inherent cross-terms and spurious events present in the quadratic time-frequency distribution. For the stability of the AR model and to make it more robust, we employed Burg's algorithm for segments in which all the kernel sequences were exploited simultaneously to compute the prediction error operator. To check the validity of this method for the ultrasonic Lamb waves, the numerical and experimental analyses were performed to generate waves in an aluminium plate for damage localization and quantification. Since inherent dispersion behaviour and multimodal nature of Lamb waves making the interpretation of the signal extremely difficult for the NDT applications, the proposed algorithm has been proved to be effective in expressing the true time-frequency energy distribution of the damage signal. The proposed scheme precisely estimated the distance between the two closely spaced damages in a plate from simulated noisy signals with maximum uncertainty of 5%. Moreover, the method was also effective in localizing the multiple overlapping Lamb modes in the time-frequency domain. For damage quantification, three damage sensitive features, namely, energy concentration, time-frequency flux, and instantaneous frequency were extracted by the proposed maximum entropy-based Wigner-Ville time-frequency distribution of pristine and damage signals. These were obtained from the five different sets of specimens. Minimum

three sets of data were used for linear regression model training and a maximum of two sets for model testing. The results show that the damage indices obtained from the proposed time-frequency method has the potential to predict the crack sizes precisely and reliably. It is important to mention here that the current study used a supervised machine learning model in which the other dimensions of crack and its orientation were fixed for all sets of specimens. For a realistic case, these parameters are unknown and significantly affect the damaged signal. Future work will consider all these issues and more tests on different materials and more complex structures may be needed to validate the effectiveness of the proposed technique of signal processing.
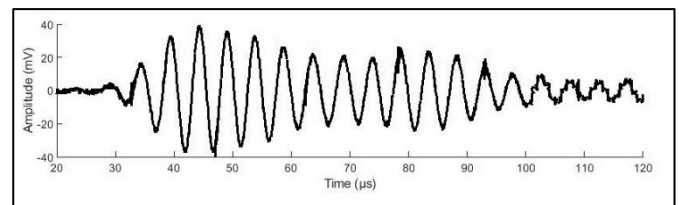

Figure 17: Original signal of 100mm crack size for first specimen.

Table 4: Experimental values of three damage indices estimated through the proposed time-frequency technique for 100mm crack sizes.

EC	TFF	IF	Predicted value	Percentage Error
0.1789	0.1589	1.3906	97.297	2.71%
0.1795	0.1517	1.3515	90.213	9.79%
0.1803	0.1571	1.4471	102.850	2.85%

8. Acknowledgement:

9. References:

[1]   Giurgiutiu V 2007 *Structural Health Monitoring with Piezoelectric Wafer Active Sensors: with Piezoelectric Wafer Active Sensors* (Elsevier)

[2]   Khan S Z, Khan M A, Tariq M, Khan K A, Khan T M and Ali T 2017 Response of Gaussian-modulated guided wave in aluminum: An analytical, numerical, and experimental study *Proc. Inst. Mech. Eng. Part C J. Mech. Eng. Sci.* **231** 3057–65

[3]   Abbas M and Shafiee M 2018 Structural health monitoring (SHM) and determination of surface defects in large metallic structures using ultrasonic guided waves *Sensors* **18** 3958

[4]   Gopalakrishnan N 2019 Piezoelectric sensor–based damage progression in concrete through serial/parallel multi-sensing technique *Struct. Heal. Monit.* **1** 18

[5]   Giurgiutiu V 2003 Lamb wave generation with piezoelectric wafer active sensors for structural health monitoring *Smart Structures and Materials 2003: Smart Structures and Integrated Systems* vol 5056 (International Society for Optics and Photonics) pp 111–23

[6]   Su Z and Ye L 2009 *Identification of damage using Lamb waves: from fundamentals to applications* vol 48 (Springer Science & Business Media)

[7]   Niethammer M, Jacobs L J, Qu J and Jarzynski J 2000 Time-frequency representation of Lamb waves using the reassigned spectrogram *J. Acoust. Soc. Am.* **107** L19–24

[8]   Wilcox P D 2003 A rapid signal processing technique to remove the effect of dispersion from guided wave signals *IEEE Trans. Ultrason. Ferroelectr. Freq. Control* **50** 419–27

[9]   Yang Y, Zhang W, Peng Z and Meng G 2012 Multicomponent signal analysis based on polynomial chirplet transform *IEEE Trans. Ind. Electron.* **60** 3948–56

[10]   Xu C, Yang Z, Chen X, Tian S and Xie Y 2018 A guided wave dispersion compensation method based on compressed sensing *Mech. Syst. Signal Process.* **103** 89–104

[11]   Zhao M, Zeng L, Lin J and Wu W 2014 Mode identification and extraction of broadband ultrasonic guided waves *Meas. Sci. Technol.* **25** 115005

[12]   Liu Z, Xu K, Li D, Ta D and Wang W 2019 Automatic mode extraction of ultrasonic guided waves using synchrosqueezed wavelet transform *Ultrasonics* **99** 105948

[13]   Chen S, Wang K, Peng Z, Chang C and Zhai W 2020 Generalized dispersive mode decomposition: Algorithm and applications *J. Sound Vib.* 115800

[14]   Cohen L 1995 *Time-frequency analysis* vol 778 (Prentice hall)

[15]   Prosser W H, Seale M D and Smith B T 1999 Time-frequency analysis of the dispersion of Lamb modes *J. Acoust. Soc. Am.* **105** 2669–76

[16]   Choi H-I and Williams W J 1989 Improved time-frequency representation of multicomponent signals using exponential kernels *IEEE Trans. Acoust.* **37** 862–71

[17]   Hu Y, Zhu Y, Tu X, Lu J and Li F 2019 Dispersion curve analysis method for Lamb wave mode separation *Struct. Heal. Monit.* 1475921719890590

[18]   Dai D and He Q 2014 Structure damage localization with ultrasonic guided waves based on a time–frequency method *Signal Processing* **96** 21–8

[19]   Hartono D, Halim D and Wyn Roberts G 2018 Gear fault diagnosis using an improved reassigned smoothed pseudo Wigner-Ville distribution *Cogent Eng.* **5** 1436928

[20]   Hamstad M A 2008 Comparison of wavelet transform and Choi-Williams distribution to determine group velocities for different acoustic emission sensors *J. Acoust. Emiss* **26** 40–59

[21]   Ono K 2017 On the piezoelectric detection of guided ultrasonic waves *Materials (Basel).* **10** 1325

[22]   Trochidis A, Hadjileontiadis L and Zacharias K 2014 Analysis of vibroacoustic modulations for crack

detection: a time-frequency approach based on zhao-atlas-marks distribution *Shock Vib.* **2014**

[23]   Tan J L and Sha'ameri A Z 2009 Adaptive optimal kernel smooth-windowed Wigner-Ville distribution for digital communication signal *EURASIP J. Adv. Signal Process.* **2008** 1–17

[24]   Auger F, Flandrin P, Gonçalvès P and Lemoine O 1996 Time-frequency toolbox *CNRS Fr. Univ.* **46**

[25]   Burg J P 1972 The relationship between maximum entropy spectra and maximum likelihood spectra *Geophysics* **37** 375–6

[26]   Zoukaneri I and Porsani M J 2015 A combined Wigner-Ville and maximum entropy method for high-resolution time-frequency analysis of seismic data *Geophysics* **80** O1–11

[27]   Wang Y, Rao Y and Xu D 2020 Multichannel maximum-entropy method for the Wigner-Ville distribution *Geophysics* **85** V25–31

[28]   Andersen N 1974 On the calculation of filter coefficients for maximum entropy spectral analysis *Geophysics* **39** 69–72

[29]   De Waele S and Broersen P M T 2000 The Burg algorithm for segments *IEEE Trans. Signal Process.* **48** 2876–80

[30]   Boashash B 2003 *Time Frequency Analysis* (Elsevier Science)

[31]   Feng Z, Liang M and Chu F 2013 Recent advances in time–frequency analysis methods for machinery fault diagnosis: A review with application examples *Mech. Syst. Signal Process.* **38** 165–205

[32]   Qian S 2002 *Introduction to Time-frequency and Wavelet Transforms* (Prentice Hall PTR)

[33]   Kumar R, Zhao W and Singh V 2018 Joint time-frequency analysis of seismic signals: A critical review *Struct. Durab. Heal. Monit* **12** 77–95

[34]   Yuchao M, Weiming Y, Haoxiang H and Kai W 2014 Damage detection based on cross-term extraction from bilinear time-frequency distributions *Math. Probl. Eng.* **2014**

[35]   Boashash B 2015 *Time-frequency signal analysis and processing: a comprehensive reference* (Academic Press)

[36]   Chen C 1988 *Signal processing handbook* vol 51 (CRC Press)

[37]   Stanković L 2001 A measure of some time–frequency distributions concentration *Signal Processing* **81** 621–31

[38]   Yang C, Ye L, Su Z and Bannister M 2006 Some aspects of numerical simulation for Lamb wave propagation in composite laminates *Compos. Struct.* **75** 267–75

[39]   Alkassar Y, Agarwal V K and Alshrihi E 2017 Simulation of Lamb wave modes conversions in a thin plate for damage detection *Procedia Eng.* **173** 948–55

[40]   Moser F, Jacobs L J and Qu J 1999 Modeling elastic wave propagation in waveguides with the finite element method *Ndt E Int.* **32** 225–34

[41]   Aharamuthu K and Ayyasamy E P 2013 Application of discrete wavelet transform and Zhao-Atlas-Marks transforms in non stationary gear fault diagnosis *J. Mech. Sci. Technol.* **27** 641–7

[42]   Hong J-C, Sun K H and Kim Y Y 2005 The matching pursuit approach based on the modulated Gaussian pulse for efficient guided-wave damage inspection *Smart Mater. Struct.* **14** 548

[43]   Boashash B, Khan N A and Ben-Jabeur T 2015 Time–frequency features for pattern recognition using high-resolution TFDs: A tutorial review *Digit. Signal Process.* **40** 1–30

[44]   He J, Guan X, Peng T, Liu Y, Saxena A, Celaya J and Goebel K 2013 A multi-feature integration method for fatigue crack detection and crack length estimation in riveted lap joints using Lamb waves *Smart Mater. Struct.* **22** 105007